EurJIC European Journal of Inorganic Chemistry
ChemPubSoc Europe
FULL PAPER

DOI:10.1002/ejic.201402563

# Effects of Ultrasonic Agitation on the Structural and Magnetic Properties of $CoFe_2O_4$ Nanocrystals

**Anielle Christine Almeida Silva,*[a] Xavier Gratens,[b] Valmir Antonio Chitta,[b] Sinésio Domingues Franco,[c] Ricardo Souza da Silva,[d] José Fernando Condeles,[d] and Noelio Oliveira Dantas*[a]**

**Keywords:** $CoFe_2O_4$ nanocrystals / Nanostructures / Annealing temperature / Ultrasonic agitation / Magnetic properties

Cobalt ferrite nanocrystals ($CoFe_2O_4$) were synthesized by means of ultrasonic agitation and afterward subjected to different annealing temperatures. The structural and morphological properties of the nanocrystals were investigated by means of X-ray diffraction and scanning electron microscopy. The results showed that the samples were composed of $CoFe_2O_4$ monophase nanocrystals. The particle size increased with increasing annealing temperatures. Infrared spectroscopy and magnetization showed that the samples exhibited the usual features of $CoFe_2O_4$ nanocrystals. Superparamagnetism was not observed at room temperature. However, the results indicated that the samples could be considered single-domain particles with blocking temperatures greater than 300 K. Both infrared and magnetic results indicated possible diffusion of cobalt ions from tetrahedral to octahedral sites as a function of the annealing temperature.

## Introduction

Magnetic nanoparticles (NPs) have unique magnetic properties such as superparamagnetism, high coercivity, and high magnetic susceptibility, which raises the possibility of their use in a broad range of applications.[1] These applications include magnetic fluids, data storage, and bioapplications.[2–4] In addition, when magnetic NPs are inserted into glass systems, it permits the generation of magneto-optical properties, which are promising in device applications that emphasize the use of the Faraday effect for magneto-optical components.[5,6] Furthermore, particularly interesting are cubic ferrite nanocrystals (NCs) of the spinel formula [$xFe_2O_4$ (e.g., X: $Co^{2+}$)] in which $O^{2-}$ ions are organized in the cubic structure and $Fe^{2+}$ or $Co^{2+}$ can occupy the tetrahedral and octahedral sites. The magnetic properties of these NCs can be controlled by the distribution of cations among the octahedral and tetrahedral sites of the spinel structure. In addition, cation distribution can depend on the synthesis method and size of the NCs. Cobalt ferrite NCs in particular exhibit high coercivity, moderate saturation magnetization, large anisotropy, light-induced changes in coercivity,[7] strong, site-specific binding of proteins in albumin serum,[8–11] high stability up to 1000 °C, high durability, and good electrical insulation properties.[12–14] Consequently, these NCs can be used in data storage,[15] ionic fluids,[16] sensors,[17,18] and drug-delivery systems for biological labeling.[19,20] Various methods are used to synthesize these NCs including hydrothermal,[21] high-temperature decomposition of organic precursors,[22] sol–gel,[23] coprecipitation,[24] microemulsion,[25] aerosol vapor,[2] Langmuir–Blodgett,[26] mechanical grinding,[27] micellar,[28] and bacterial synthesis.[29] The coprecipitation method is based on nanocrystal nucleation and subsequent growth. Nucleation and growth control the final shape of the nanocrystals and are strongly affected by various parameters such as agitation speed, synthesis temperature, the nature of alkaline solutions, addition rate, digestion time, and pH.[30,31] Therefore, coprecipitation is one of the most versatile techniques. Our study is probably the first to use ultrasonic agitation in aqueous solution throughout the entire process of synthesizing cobalt ferrite NCs. Ultrasonic agitation favors the formation of uniformly sized, highly magnetized cobalt ferrite nanocrystals. This fact deserves special attention because, according to the literature, cobalt ferrite nanocrystals obtained by coprecipitation have lower magnetism than

[a] Laboratório de Novos Materiais Isolantes e Semicondutores (LNMIS), Instituto de Física, Universidade Federal de Uberlândia,
Uberlândia, Brasil
E-mail: aniellechristine@yahoo.com.br
noelio@ufu.br
http://www.lnmis.infis.ufu.br/
[b] Laboratório de Estado Sólido e Baixas Temperaturas, Instituto de Física, Universidade de São Paulo,
São Paulo, Brasil
[c] Laboratório de Tecnologia em Atrito e Desgaste (LTAD), Faculdade de Engenharia Mecânica, Universidade Federal de Uberlândia,
Uberlândia, Brasil
[d] Universidade Federal do Triângulo Mineiro, Instituto de Ciências Exatas, Naturais e Educação (ICENE), Departamento de Física,
Uberaba, Brasil

those obtained by our methodology.[24,32,33] We confirmed these results by means of X-ray diffraction, scanning electron microscopy, IR spectroscopy, and magnetization measurements.

## Results and Discussion

The XRD patterns of the AN300, AN600, and AN900 samples (annealed at 300, 600, and 900 °C, respectively) are shown in Figure 1. The diffraction peaks for all samples agree with the diffraction pattern of the cubic spinel structure of $CoFe_2O_4$ (JCPDS card no. 22–1086).[34] The absence of additional peaks indicates the high purity of the $CoFe_2O_4$ phase. The average particle sizes ($D$) were determined by using the Debye–Scherrer equation and the full width at half-maximum (FWHM) of the most intense peak (3 1 1), see Equation (1).[35]

$$D = 0.9\lambda/\beta\cos\theta \quad (1)$$

$\lambda$ is the radiation wavelength, $\beta$ is the FWHM, and $\theta$ represents the diffraction of the peak. We obtained $D$ = 13, 18, and 40 nm for the AN300, AN600, and AN900 samples, respectively. The observed increase in the NC size with increasing annealing temperature is related to the interdependence between the different rates of nucleation and growth in ferrite formation.[18] Thus, higher annealing temperatures decrease structure defects, improve crystallinity, and cause crystallite coalescence, which increases the size of the $CoFe_2O_4$ NCs.[36]

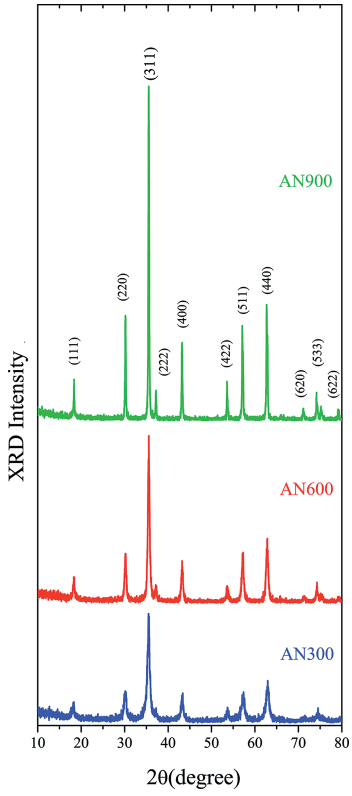


Figure 1. X-ray diffraction patterns of the AN300, AN600, and AN900 samples.

Field-emission gun scanning electron microscopy (FEG-SEM) images of the $CoFe_2O_4$ NCs from the AN300, AN600, and AN900 samples are shown in Figure 2 (a–c), respectively. The images show that the NCs are spherical, uniform, monodisperse, and uniformly sized. The observed sizes of the NCs in the expanded view of the SEM images are in good agreement with those calculated from the XRD data. The spherical shape of these particles is probably due to the non-use of surfactant.[37] The results displayed in Figure 2 shows NC clustering, which is associated with van der Waals forces between nanocrystals and strong magnetic interactions.[38] This effect is greater with increasing annealing temperature, since the increase in the annealing temperatures also favors $CoFe_2O_4$ NC clustering.

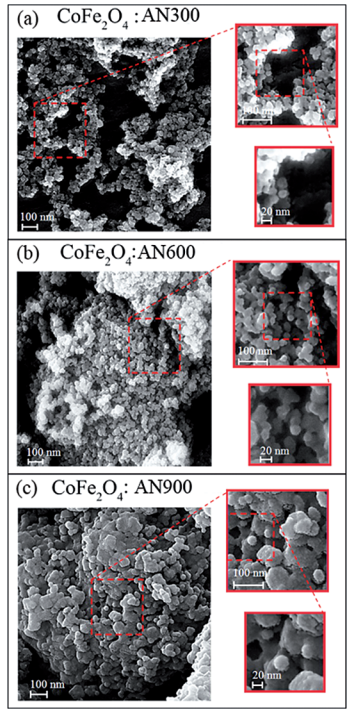


Figure 2. FEG-SEM images of $CoFe_2O_4$ NCs from the AN300, AN600, and AN900 samples.

The FTIR spectra of the samples are shown in Figure 3. Two bands at 400–450 ($\nu_2$) and 550–650 ($\nu_1$) $cm^{-1}$ are typical of a spinel ferrite (see Figure 3).[39] The higher-frequency band ($\nu_1$) is caused by intrinsic stretching vibrations at tetrahedral sites (Fe–O or Co–O vibrations) in the metal. The lower-frequency band ($\nu_2$) corresponds to octahedral metal stretching.[39] The positions of these bands confirm the formation of cobalt ferrite NPs.[40] The increase in the $\nu_1$ absorption band intensity with increasing annealing temperature is attributed to greater local order and crystallinity, which is in agreement with the XRD results.[41] The FTIR spectra of the ferrite might also provide information on the cation distribution over the tetrahedral (Td) and octahedral (Oh) sites. Previous studies have shown that increasing annealing temperatures causes $\nu_1$ and $\nu_2$ bands to shift to lower frequencies.[25,41] These shifts are attributed to changes in cation distribution and variations in the length

of cation–oxygen bonds at Td and Oh sites. The bands associated with the $\nu_1$ and $\nu_2$ frequencies shift to lower frequencies as the annealing temperature increases, thereby confirming that $Co^{+2}$ ions are incorporated into the Oh sites. This is justified because the increase in site radius reduces the fundamental frequency and thus the center of the bands must shift to lower frequencies.[40] In addition, $\nu_2$ band intensity increases with higher annealing temperatures, which also confirms incorporation of the $Co^{+2}$ ion into Oh sites. On the basis of these results, we concluded that increasing the annealing temperature causes the diffusion of $Co^{+2}$ ions from Td to Oh sites.

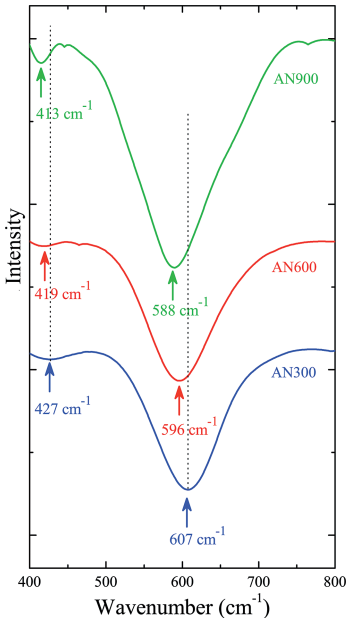


Figure 3. FTIR spectra of the $CoFe_2O_4$ NCs for the AN300, AN600, and AN900 samples.

The magnetization ($M$) versus applied magnetic field ($H$) curves obtained at 300 K for the three samples are shown in Figure 4. The saturation magnetization ($M_S$) value was determined by fitting the high-field segment of the $M/H$ virgin curve using Equation (2)[42] in which $a$ and $b$ are fitting parameters.

$$M/M_S = 1 - a/H - b/H^2 \quad (2)$$

The obtained $M_S$ values show that the magnetization at 65 kOe is near saturation for all three samples (Table 1). The value of $M$ measured at 65 kOe represents about 95% of $M_S$ for each sample. The obtained $M_S$ values for the three samples are lower than the bulk value $M_S$ = 80.8 emu g$^{-1}$.[43] This result is usually obtained for cobalt ferrite nanocrystals. It is attributed to the contribution of particle surface spins to the magnetic properties, which becomes relevant relative to the contribution of the spins in the core for small particles. Different magnetic states for the surface spins can lead to surface spin disorder or a canting effect.[44,45] The contribution of the surface spins (compared to the core spins) increases with decreasing particle size,

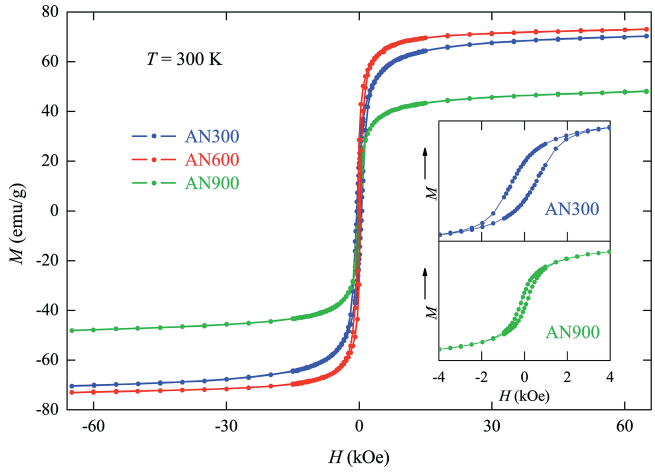


Figure 4. Magnetization versus applied magnetic field measured at 300 K for $CoFe_2O_4$ NCs for the AN300, AN600, and AN900 samples, respectively. Both inset graphs show an enlarged view of the $M/H$ loops at $H$ = 0 for AN300 and AN600, respectively.

thus leading to a decrease in $M_S$ as a function of the particle size. The $M/H$ loops measured for a field up to 65 kOe clearly show that the three samples are ferromagnetic at 300 K with remanence and coercivity ($H_C$) (see Table 1 for the $H_C$ values). In addition, hysteresis narrows as the particle size increases.

Table 1. Magnetic parameters of the samples annealed at 300 °C (AN300), 600 °C (AN600), and 900 °C (AN900). $T_B$(5 kOe) is the blocking temperature determined from the zero-field cooling experiments performed at 5 kOe. $M_S$ is the saturation magnetization value determined from the $M/H$ data, and $H_C$ is the coercivity.

| Sample | 300 K | | 1.7 K | | $T_B$(5 kOe) |
|---|---|---|---|---|---|
| | $M_S$ [emu g$^{-1}$] | $H_C$ [Oe] | $M_S$ [emu g$^{-1}$] | $H_C$ | |
| AN300 | 72.4 | 555 | 84 | 14 kOe | 260 K |
| AN600 | 74.4 | 245 | 88 | 335 Oe | 260 K |
| AN900 | 50.4 | 136 | 61 | 255 Oe | 210 K |

Superparamagnetic behavior in the samples was investigated by measuring magnetization as a function of the zero-field cooling (ZFC) and field cooling (FC) temperatures. The data displayed in Figure 5 were obtained under a 5 kOe magnetic field. Clear irreversibility between the ZFC and FC curves was observed for all three samples. When the temperature decreased from 300 to 2 K, the ZFC curve reached a maximum and then decreased rapidly, whereas the FC curve increased slightly. This maximum is observed at a critical temperature called the blocking temperature $T_B$(5 kOe) at $H$ = 5 kOe. The value of $T_B$(5 kOe) is near 260 K for the AN300 and AN600 samples and close to 210 K for the AN900 sample. The blocking temperature shifts to higher temperatures as the field decreases.[46] Figure 5 also shows the ZFC and FC magnetization measurements at $H$ = 500 Oe for the AN900 sample. The ZFC curve does not reach a maximum, and the ZFC and FC traces do not overlap. Similar results were obtained for the AN300

 

and AN600 samples. Overall, these results provide convincing evidence that the samples possess superparamagnetic properties with blocking temperatures $T_B$ ($H \rightarrow 0$) that exceed 300 K.

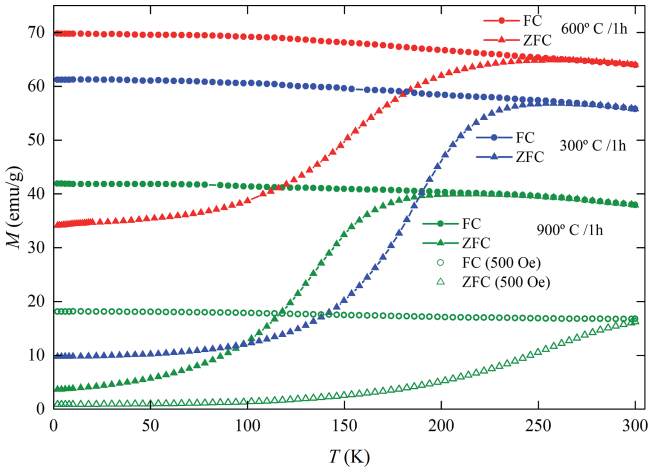


Figure 5. Field cooling (FC) and zero-field cooling (ZFC) temperature variation of magnetization measured at 5 kOe (solid symbols) for the three samples. Data obtained at 500 Oe for the AN900 sample are also displayed. Only the high-temperature segment of the FC curve is shown for a better overall view of the experimental results.

The $M/H$ loops measured for a magnetic field up to 65 kOe at $T$ = 1.7 K for the AN300, AN600, and AN900 samples are shown in Figure 6. The saturation magnetization of the three samples increases as temperature decreases. The obtained values for $M_S$ are lower than the bulk $M_S$ = 93.9 emu g$^{-1}$ value.[43] The magnetization curve of the AN300 sample consists of a large hysteresis loop ($H_C$ = 14 kOe) and a rapid change in $M$ near the zero applied magnetic field. This kind of constricted hysteresis loop has been observed in other studies on $CoFe_2O_4$ nanocrystals and has been attributed to strong dipolar interparticle interaction.[47,48] The observed shape of the $M/H$ loop can be also obtained for a mixture of soft and hard magnetic materials. On the basis of the present data, this possibility cannot be ruled out. The constricted hysteresis loop is not observed for the two other samples. In addition, the $M/H$ loops for samples AN600 and AN900 show lower coercive force than sample AN300. This sample has a smaller size and a higher surface-to-volume ratio. Assuming a single magnetic phase for sample AN300, we expect that this sample has higher uncoupled spins on the surface than in the core of the particle to result in a larger surface anisotropy contribution and larger $H_C$.

The virgin $M/H$ trace was obtained at 300 K and 1.7 K ZFC for the AN900 sample. The S-shape of this trace was also observed for the other two samples and has been reported previously, as shown in Figure 7.[44] S-shaped virgin magnetization is usually observed in frustrated systems such as spin glasses and might indicate, as in the present case, the existence of competing interparticle interactions.

Overall, these magnetic results provide strong evidence that the samples consist of single-domain nanocrystals with

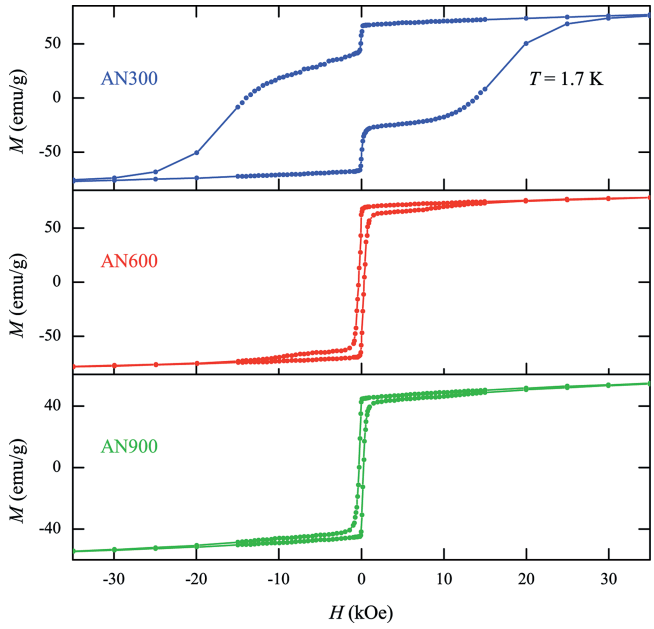


Figure 6. $M/H$ loops measured for fields up to 65 kOe at $T$ = 1.7 K for the $CoFe_2O_4$ nanocrystals in the AN300, AN600, and AN900 samples, respectively.

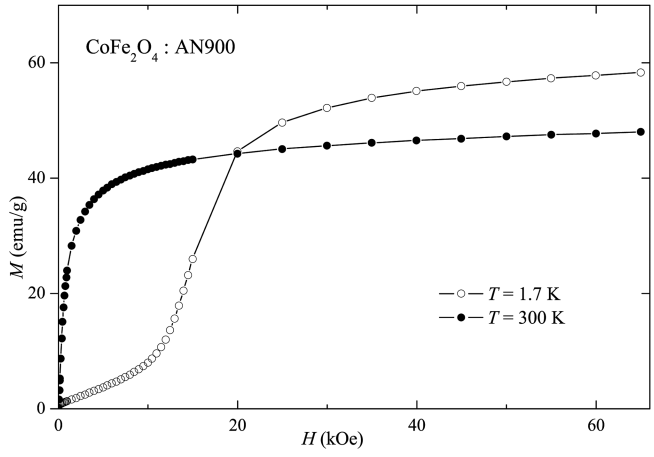


Figure 7. Virgin magnetization curves at $T$ = 300 K and $T$ = 1.7 K for the AN900 sample. The low-temperature trace was obtained after zero-field cooling of the sample.

a blocking temperature greater than room temperature. We obtained lower $M_S$ values for these samples than for the bulk. This result is generally observed for ferrite NPs and usually ascribed to surface spin disorders or spin-canting effects.[49] Size-dependent saturation magnetization is expected. The value of $M_S$ decreases with decreasing particle size. The $M_S$ values for samples AN300 and AN600 follow this pattern; however, the $M_S$ value of sample AN900, with the largest size, is clearly lower than that for the two other samples. The observed result for sample AN900 might be explained by a change in the cation distribution of Co and Fe as discussed in the following. In the spinel structure of cobalt ferrite, Co and Fe can occupy Oh and Td sites. The cation distribution can be described by the formula

 

$(Co_{1-x}Fe_x)_{Td}[Co_xFe_{2-x}]_{Oh}O_4$, in which $x$ is the degree of inversion. In normal spinels ($x$ = 0), $Co^{2+}$ ions occupy Td sites and $Fe^{3+}$ occupy Oh sites. In inverse spinels ($x$ = 1), $Co^{2+}$ ions are located at Oh sites, and $Fe^{3+}$ ions are located at Td and Oh sites. The net magnetization is the difference between the sum of the magnetic moments of cations at Oh sites and the sum of the magnetic moments of cations at Td sites. A decrease in saturation magnetization is therefore expected as $x$ increases.

Thus, the large reduction in $M_S$ for the AN900 sample is ascribed to greater changes in cation distribution (increasing $x$) relative to the other samples. Annealing at 900 °C causes a transfer of Co ions from Td sites to Oh sites and transfer of Fe ions from Oh to Td sites. This result is in agreement with those obtained from the FTIR experiments (Figure 3). The overall features of the magnetic properties of the samples agree with previous studies.[44,47,48,50]

## Conclusion

We successfully used the ultrasonic agitation technique to produce pure cubic spinel $CoFe_2O_4$ nanocrystals with a narrow size distribution. A clear correlation between the size and crystallinity of the particles and the annealing temperature was observed. Increasing the annealing temperature decreases structure defects, improves crystallinity, and increases the size of the particles without changing their shape. Our samples can be considered single-domain particles with blocking temperatures greater than room temperature. For two samples, the obtained saturation magnetization values, $M_S$, are similar to those found in other studies on similarly sized particles. In the sample with the largest particles, $M_S$ increases with increasing particle size. This behavior is unexpected and indicates that annealing might control particle size and the distribution of $Co^{+2}$ over Td and Oh sites, which is corroborated by FTIR spectroscopy measurements. We believe that these results provide a significant advance in the search for possible technological applications.

## Experimental Section

**Materials:** $CoFe_2O_4$ nanocrystals were prepared using cobalt(II) chloride ($CoCl_2$; ≥98.0%), iron(III) chloride hexahydrate ($FeCl_3{\cdot}6H_2O$; 97%), and sodium hydroxide (NaOH; ≥98.0%). All chemicals were purchased from Sigma–Aldrich.

**Synthesis of $CoFe_2O_4$ Nanocrystals:** Cobalt ferrite nanocrystals were synthesized by ultrasonic agitation during the entire process. A solution was prepared with 0.5 M cobalt(II) chloride and 1 M iron(III) chloride in aqueous solution. An 8 M NaOH solution was then added drop by drop to increase the pH of the mixed solution up to 11. This solution was heated at 90 °C for 4 h. The obtained precipitate was then purified several times using ultrapure water until reaching pH value 7. All the growth parameters, pH, $Co^{2+}$/$Fe^{3+}$ molar ratio, reaction temperature, and NaOH concentration were controlled to improve the formation of pure-phase $CoFe_2O_4$. Finally, the precipitate was annealed under an ambient atmosphere at 300, 600, and 900 °C for 1 h. The obtained samples were labeled AN300, AN600, and AN900, respectively.

**Sample Characterization:** The structural phase of the samples was investigated using X-ray diffraction (XRD) patterns obtained at room temperature with an XRD-6000 Shimadzu diffractometer with monochromatic Cu-$K_{\alpha 1}$ radiation ($\lambda$ = 1.54056 Å). The morphology of the samples was studied by FEG-SEM with a Zeiss microscope at 10 kV. IR spectra of the samples were recorded at room temperature using the transmission mode of a Shimadzu Fourier transform IR (FTIR) spectrophotometer (model IR Prestige-21) in the 450 to 4600 $cm^{-1}$ spectral range). Magnetization measurements were performed with a Cryogenics S600 superconducting quantum interference device (SQUID) magnetometer in the temperature range from 1.7 to 300 K and magnetic field up to 65 kOe.

## Acknowledgments

The authors gratefully acknowledge financial support by the Coordenação de Aperfeiçoamento de Pessoal de Nível Superior, Fundação de Amparo à Pesquisa do Estado de Minas Gerais (CAPES, FAPEMIG), the Conselho Nacional de Desenvolvimento Científico e Tecnológico (MCT/CNPq), and by NANOBIOTEC BRAZIL. The authors are also grateful for the use of the Shimadzu FTIR spectrophotometer (model IR Prestige-21) with support from Shimadzu Brazil and for the use of the XRD-6000 diffractometer (Shimadzu) at the Institute of Chemistry, Federal University of Uberlândia (UFU), with financial support by the Coordenação de Aperfeiçoamento de Pessoal de Nível Superior (CAPES) ("Pró-Equipamentos" grant). The technician and operator Flávio Alves dos Santos is thanked for the production of the SEM images with the FEG-SEM supported by PETROBRAS.

[1] W. Wu, Q. G. He, C. Z. Jiang, *Nanoscale Res. Lett.* **2008**, *3*, 397–415.
[2] S. Laurent, D. Forge, M. Port, A. Roch, C. Robic, L. V. Elst, R. N. Muller, *Chem. Rev.* **2008**, *108*, 2064–2110.
[3] T. K. Jain, M. A. Morales, S. K. Sahoo, D. L. Leslie-Pelecky, V. Labhasetwar, *Mol. Pharm.* **2005**, *2*, 194–205.
[4] M. Calero, L. Gutierrez, G. Salas, Y. Luengo, A. Lazaro, P. Acedo, M. P. Morales, R. Miranda, A. Villanueva, *Nanomedicine (N. Y., NY, U. S.)* **2014**, *10*, 733–743.
[5] N. O. Dantas, W. E. F. Ayta, A. C. A. Silva, N. F. Cano, A. F. R. Rodriguez, A. C. Oliveira, V. K. Garg, P. C. Morais, *Solid State Sci.* **2012**, *14*, 1169–1174.
[6] N. O. Dantas, W. E. F. Ayta, A. C. A. Silva, N. F. Cano, S. W. Silva, P. C. Morais, *Spectrochim. Acta Part A* **2011**, *81*, 140–143.
[7] B. D. Cullity, C. D. Graham, *Introduction to Magnetic Materials*, Wiley-IEEE Press, **2008**.
[8] P. C. Morais, *J. Alloys Compd.* **2009**, *483*, 544–548.
[9] H. M. Joshi, Y. P. Lin, M. Aslam, P. V. Prasad, E. A. Schultz-Sikma, R. Edelman, T. Meade, V. P. Dravid, *J. Phys. Chem. C* **2009**, *113*, p. 17761–17767.
[10] S. Kuckelhaus, V. A. P. Garcia, L. M. Lacava, R. B. Azevedo, Z. G. M. Lacava, E. C. D. Lima, F. Figueiredo, A. C. Tedesco, P. C. Morais, *J. Appl. Phys.* **2003**, *93*, 6707–6708.
[11] Q. A. Pankhurst, J. Connolly, S. K. Jones, J. Dobson, *J. Phys. D* **2003**, *36*, R167–R181.
[12] O. Song, Z. J. Zhang, *J. Am. Chem. Soc.* **2004**, *126*, 6164–6168.
[13] S. Ayyappan, S. Mahadevan, P. Chandramohan, M. P. Srinivasan, J. Philip, B. Raj, *J. Phys. Chem. C* **2010**, *114*, 6334–6341.
[14] D. Peddis, M. V. Mansilla, S. Morup, C. Cannas, A. Musinu, G. Piccaluga, F. D'Orazio, F. Lucari, D. Fiorani, *J. Phys. Chem. B* **2008**, *112*, 8507–8513.

 

[15] A. K. Giri, E. M. Kirkpatrick, P. Moongkhamklang, S. A. Majetich, V. G. Harris, *Appl. Phys. Lett.* **2002**, *80*, 2341–2343.
[16] P. C. Morais, V. K. Garg, A. C. Oliveira, L. P. Silva, R. B. Azevedo, A. M. L. Silva, E. C. D. Lima, *J. Magn. Magn. Mater.* **2001**, *225*, 37–40.
[17] J. A. Paulsen, A. P. Ring, C. C. H. Lo, J. E. Snyder, D. C. Jiles, *J. Appl. Phys.* **2005**, *97*.
[18] C. N. Chinnasamy, B. Jeyadevan, O. Perales-Perez, K. Shinoda, K. Tohji, A. Kasuya, *IEEE Trans. Magn.* **2002**, *38*, 2640–2642.
[19] R. Banerjee, Y. Katsenovich, L. Lagos, M. McIintosh, X. Zhang, C. Z. Li, *Curr. Med. Chem.* **2010**, *17*, 3120–3141.
[20] D. B. Robinson, H. H. J. Persson, H. Zeng, G. X. Li, N. Pourmand, S. H. Sun, S. X. Wang, *Langmuir* **2005**, *21*, 3096–3103.
[21] L. J. Zhao, H. J. Zhang, Y. Xing, S. Y. Song, S. Y. Yu, W. D. Shi, X. M. Guo, J. H. Yang, Y. Q. Lei, F. Cao, *J. Solid State Chem.* **2008**, *181*, 245–252.
[22] T. Hyeon, Y. Chung, J. Park, S. S. Lee, Y. W. Kim, B. H. Park, *J. Phys. Chem. B* **2002**, *106*, 6831–6833.
[23] G. B. Ji, S. L. Tang, B. L. Xu, B. X. Gu, Y. W. Du, *Chem. Phys. Lett.* **2003**, *379*, 484–489.
[24] Y. I. Kim, D. Kim, C. S. Lee, *Phys. B* **2003**, *337*, 42–51.
[25] S. Ammar, A. Helfen, N. Jouini, F. Fievet, I. Rosenman, F. Villain, P. Molinie, M. Danot, *J. Mater. Chem.* **2001**, *11*, 186–192.
[26] T. Meron, Y. Rosenberg, Y. Lereah, G. Markovich, *J. Magn. Magn. Mater.* **2005**, *292*, 11–16.
[27] E. Manova, B. Kunev, D. Paneva, I. Mitov, L. Petrov, C. Estournes, C. D'Orleans, J. L. Rehspringer, M. Kurmoo, *Chem. Mater.* **2004**, *16*, 5689–5696.
[28] S. Rana, J. Philip, B. Raj, *Mater. Chem. Phys.* **2010**, *124*, 264–269.
[29] V. S. Coker, N. D. Telling, G. van der Laan, R. A. D. Pattrick, C. I. Pearce, E. Arenholz, F. Tuna, R. E. P. Winpenny, J. R. Lloyd, *Acs Nano* **2009**, *3*, 1922–1928.
[30] S. Ayyappan, J. Philip, B. Raj, *J. Phys. Chem. C* **2009**, *113*, 590–596.
[31] F. A. Tourinho, R. Franck, R. Massart, *J. Mater. Sci.* **1990**, *25*, 3249–3254.
[32] S. Briceno, W. Bramer-Escamilla, P. Silva, G. E. Delgado, E. Plaza, J. Palacios, E. Canizales, *J. Magn. Magn. Mater.* **2012**, *324*, 2926–2931.
[33] M. A. G. Soler, E. C. D. Lima, S. W. da Silva, T. F. O. Melo, A. C. M. Pimenta, J. P. Sinnecker, R. B. Azevedo, V. K. Garg, A. C. Oliveira, M. A. Novak, P. C. Morais, *Langmuir* **2007**, *23*, 9611–9617.
[34] F. Cardarelli, *Materials Handbook: A Concise Desktop Reference*, Springer London, **2008**.
[35] B. D. Cullity, *Elements of X-ray Diffraction*, BiblioBazaar, **2011**.
[36] T. P. Raming, A. J. A. Winnubst, C. M. van Kats, A. P. Philipse, *J. Colloid Interface Sci.* **2002**, *249*, 346–350.
[37] H. L. Yuan, Y. Q. Wang, S. M. Zhou, L. S. Liu, X. L. Chen, S. Y. Lou, R. J. Yuan, Y. M. Hao, N. Li, *Nanoscale Res. Lett.* **2010**, *5*, 1817–1821.
[38] J. D. Gomes, M. H. Sousa, F. A. Tourinho, R. Aquino, G. J. da Silva, J. Depeyrot, E. Dubois, R. Perzynski, *J. Phys. Chem. C* **2008**, *112*, 6220–6227.
[39] R. D. Waldron, *Phys. Rev.* **1955**, *99*, 1727–1735.
[40] R. C. Kambale, K. M. Song, Y. S. Koo, N. Hur, *J. Appl. Phys.* **2011**, *110*, 053910–053910–053917.
[41] L. Kumar, P. Kumar, A. Narayan, M. Kar, *Int. Nano Lett.* **2013**, *3*, 1–12.
[42] A. H. Morrish, *The Physical Principles of Magnetism*, Wiley, **1965**.
[43] M. Grigorova, H. J. Blythe, V. Blaskov, V. Rusanov, V. Petkov, V. Masheva, D. Nihtianova, L. M. Martinez, J. S. Muñoz, M. Mikhov, *J. Magn. Magn. Mater.* **1998**, *183*, 163–172.
[44] D. Peddis, N. Yaacoub, M. Ferretti, A. Martinelli, G. Piccaluga, A. Musinu, C. Cannas, G. Navarra, J. M. Greneche, D. Fiorani, *J. Phys. Condens. Matter* **2011**, *23*, 426004.
[45] R. H. Kodama, A. E. Berkowitz, E. J. McNiff, S. Foner, *Phys. Rev. Lett.* **1996**, *77*, 394–397.
[46] V. Blaskov, V. Petkov, V. Rusanov, L. M. Martinez, B. Martinez, J. S. Muñoz, M. Mikhov, *J. Magn. Magn. Mater.* **1996**, *162*, 331–337.
[47] L. B. Tahar, L. S. Smiri, M. Artus, A. L. Joudrier, F. Herbst, M. J. Vaulay, S. Ammar, F. Fiévet, *Mater. Res. Bull.* **2007**, *42*, 1888–1896.
[48] M. Coskun, M. M. Can, O. D. Coskun, M. Korkmaz, T. Firat, *J. Nanopart. Res.* **2012**, *14*.
[49] M. P. Rajendran, R. C. Pullar, A. K. Bhattacharya, D. Das, S. N. Chintalapudi, C. K. Majumdar, *J. Magn. Magn. Mater.* **2001**, *232*, 71–83.
[50] K. Maaz, A. Mumtaz, S. K. Hasanain, A. Ceylan, *J. Magn. Magn. Mater.* **2007**, *308*, 289–295.

Received: June 18, 2014
Published Online: October 8, 2014

 